Zinc Loss Inhibition in Phosphorus-Doped Zinc-Based Core-Shell Catalysts for Vinyl Acetate Synthesis

Yilei Feng, Peng Ren, Dashun Lu, Hao Jiang, Ruyue Tan, Xugen Wang*, Bin Dai*
School of Chemistry and Chemical Engineering, Shihezi University, Shihezi, Xinjiang, China
**Corresponding Author.*

Abstract: A phosphorus-incorporated, zinc-based core-shell catalyst was synthesized via an in situ method for selective coating. The catalyst showed excellent activity and stability for the vinyl acetate synthesis. Results indicated that the optimal activity (53%) was achieved when adding 5% of HEDP (Etidronic acid) to the RF solution during the core-shell preparation, followed by calcination at 650℃. Characterization showed that the addition of HEDP decreased the electron cloud density around Zn, enhancing the adsorption of acetic acid and reducing the adsorption of acetylene, which facilitated the reaction and improved the conversion rate of acetic acid. A stability test over 550 h showed that the activity decreased by about 3%; the Zn loss rate was 6.29% (0.011%/h). The loss rate for the catalysts without a phosphorous source and with HEDP was 0.031%/h and 0.025%/h, respectively. This indicates that the addition of HEDP effectively mitigates the Zn loss rate.

Keywords: Origin of Generation; HEDP; Zn Loss; Core-shell Catalyst

1. Introduction

Vinyl acetate (VAc) is a critical chemical raw material widely used in the production of various important chemical products, such as polyvinyl alcohol, polyvinyl acetate, and acetal resins [1]. VAc can be synthesized through either the ethylene or acetylene method. Compared to the ethylene method, the latter offers several advantages, including a simpler process, lower infrastructure costs, and the use of readily available catalysts. Given the distribution of resources in China, the calcium carbide–acetylene process holds great potential for further development. However, the industrial use of zinc acetate-activated carbon catalysts presents certain challenges, including its limited lifespan and susceptibility to deactivation. To improve the efficiency and economic viability of the process, further improvements in catalyst structural design are required. Previous studies have revealed the negative impact of Zn loss on the catalyst lifespan and stability, with such deactivation being irreversible. Minimizing the loss of active components remains a crucial research area. Various methods, including the use of complexing agents [2], atomic layer deposition (ALD) [3], metal–organic frameworks (MOFs) [4], and core-shell structured materials, have been explored to address such challenges.

Core-shell structured catalysts represent a novel type of catalytic materials [5,6]. They offer a unique catalytic environment where the synergistic effect between the core and the shell can effectively regulate both the activity and selectivity of the reaction. Recent studies indicate that the treatment of porous carbon materials with phosphoric acid can increase the specific surface area of the catalyst, significantly increasing the hydroxyl group content and reducing the carboxyl group proportion, thus enhancing the catalytic performance in the acetylene acetic acid reaction. Additionally, adding phosphotungstic acid to the catalyst can improve the zinc dispersion, suppress the zinc loss, and reduce catalyst coking [7].

In this work, we prepared zinc oxide core-shell catalysts which were selectively coated with HEDP (Etidronic acid). The coating was then carbonized to create the phosphorus-doped core-shell structure catalyst, 100 nm ZnO@HEDP-RF-C/AC (RF-C is hydroquinone polymerization, AC is Activated carbon). The composition of the catalyst was analyzed using Fourier transform infrared (FTIR) spectroscopy, X-ray diffraction (XRD), and X-ray photoelectron spectroscopy (XPS). Additionally, scanning electron microscopy

(SEM) and transmission electron microscopy (TEM) were utilized to characterize the morphology and microstructure of the catalyst. In addition, inductively coupled plasma optical emission spectroscopy (ICP–OES) was used to determine the zinc content in the catalyst. The activity and stability of the catalyst were evaluated in a fixed-bed microreactor.

2. Experimental

2.1 Materials

Bisphenol A, phosphoric acid (Pi), polyphosphate (PPA), phytic acid (PA), pyrophosphate (PPi), 2-hydroxyphosphonylacetic acid (HPAA), triphenylphosphine (PPh_3), and hydroxyethylidene diphosphonic acid (HEDP) were purchased from Shanghai Macklin Biochemical Technology Co., Ltd. Formaldehyde (37–40 wt%) was obtained from Tianjin Xinbote Chemical Co., Ltd.; zinc acetate ($Zn(CH_3COO)_2$) was from Aladdin Biochemical Technology Co., Ltd.; acetylene (99.9%) was from Shihezi Hongsheng Gas Co., Ltd.; anhydrous ethanol (CH_3CH_2OH) and acetic acid (CH_3COOH) were from Tianjin Fuyu Fine Chemical Co., Ltd.; ammonia solution (NH_3H_2O) (25–28 wt%) was from Tianjin Fengchuan Chemical Reagent Technology Co., Ltd.; and activated carbon (40–60 mesh) was from Fujian Senson AC Co., Ltd.

2.2 Characterization

SEM images were acquired using a SU8010 microscope. The infrared spectra (400–4,000 cm−1) were recorded using a Bruker Senterra spectrometer. XRD patterns were collected using a Bruker D8 ADVANCE diffractometer (Germany). Inductively coupled plasma optical emission spectroscopy (ICP–OES) data were obtained on a Antitron ICP–OES 730 instrument (USA) to quantify the zinc content. High-resolution transmission electron microscopy images were captured using a FEI Tecnai G2 F30 microscope. The adsorption capacity and strength of the catalyst toward acetic acid, acetylene, and vinyl acetate (VAc) were evaluated using an AMI-300Lite temperature-programmed desorption (TPD) system.

2.3 Preparation of the Catalyst

2.3.1. Preparation of the core-shell catalyst 100 nm ZnO@5%HEDP-RF-C

Three grams of 100 nm zinc oxide particles were dispersed in a mixed solution of 200 mL anhydrous ethanol and 100 mL deionized water, followed by ultrasound dispersion for 2 h. Ammonia was added to the solution, which was thoroughly stirred for 1 h, to adjust the pH to approximately ten. Then, 0.3 g of resorcinol and 0.16 g of HEDP were added to the mixed solution. After 30 min of stirring, 0.56 mL of the formaldehyde solution were added and the reaction was allowed to proceed for 24 h. The product was washed three times alternating anhydrous ethanol and deionized water, dried at 80°C, and purged in a tubular furnace with nitrogen at room temperature for 30 min. Afterward, the temperature was increased to 650°C at a 5°C/min rate; calcination lasted 4 h, and the carbon–phosphorus core-shell structure of 100 nm ZnO@mHEDP-RF-C-T was obtained ("m" represents the mass ratio of HEDP to ZnO, and T indicates the carbonization temperature).

2.3.2. Optimization of the HEDP incorporation sequence

A total of 3 g of 100 nm zinc oxide particles were added to a 500 mL beaker containing a mixed solution of 200 mL anhydrous ethanol and 100 mL deionized water. The mixture was ultrasonically dispersed for 2 h. Ammonia was added to adjust the pH to 9, and the mixture was stirred for 1 h. Then, 0.3 g of resorcinol was added and stirred for 30 min to ensure uniform dispersion. Next, 0.56 mL of the formaldehyde solution was added and the reaction proceeded for 24 h. The product was washed three times alternating anhydrous ethanol and deionized water, dried at 80°C, and then dissolved with 0.16 g of HEDP in 50 mL of deionized water. The mixture was allowed to react for 12 h at 80°C and then dried at 80°C. The dried product was placed in a tube furnace. Initially, the tube was purged with nitrogen gas for 30 min at room temperature to remove air. The temperature was then raised to 650°C at a rate of 5°C/min and held for 4 h to completely calcine into a carbon–phosphorus shell, named 100 nm ZnO@RF-3%HEDP-C. In a different procedure, without the addition of HEDP before calcination, the calcined product was

dissolved with 0.16 g of HEDP in 50 mL of deionized water and allowed to react for 12 h at 80°C. The dried product was named 100 nm ZnO@RF-C3%HEDP. The catalyst prepared according to the procedures in section 2.3.1 is referred to as 100 nm ZnO@3%HEDP-RF-C.

2.4 Performance Evaluation

The catalyst was evaluated in a fixed-bed microreactor. A total of 0.9 g (1.5 mL) of the catalyst was loaded into a tubular reactor, and the following operational steps were performed. The nitrogen valve was opened, and the flow rate was adjusted to 12.5 mL/min. The reactor temperature was then set to 220°C, and the acetic acid heater was set to 150°C. After approximately 30 min to allow the system to reach the set temperatures, the acetic acid peristaltic pump was activated, allowing its flow at 0.1 mL/min for 40 min to ensure complete formation of zinc acetate from zinc oxide. The nitrogen valve was then closed, and the acetylene valve was opened, setting its volume space velocity (GHSV) to 500 h^{-1} (12.5 mL/min), while the acetic acid flow rate was maintained at 0.01 mL/min. The reaction temperature was maintained at 220°C, with a 3:1 acetylene: acetic acid molar feed ratio. The performance of the samples was analyzed using gas chromatography.

3. Results and Discussion

3.1. Influence of Different Phosphorus Containing Groups on the Catalytic Activity

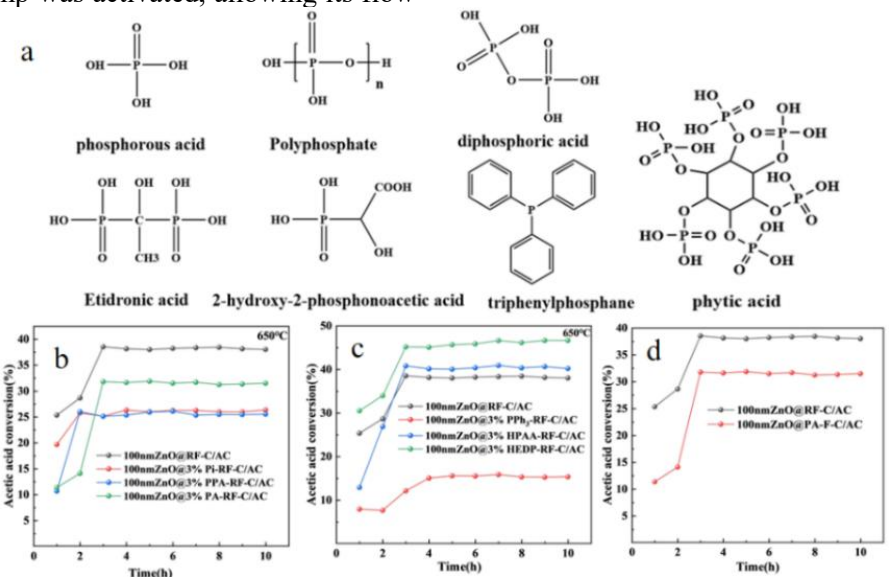

Figure 1. (a) Structure of Different Phosphorus-containing Molecules, Catalytic Performance for the Acetic Acid Conversion When Adding (b) Phosphate, (c) Phosphonic Acid Groups, and (d) Pyrophosphate Groups to the Catalyst.

Seven phosphorus sources containing phosphate, pyrophosphate, or phosphonic acid groups were selected and added to the resorcinol–formaldehyde (RF) shell material, Figure 1a. The acetic acid conversion rates for the catalysts 100 nm ZnO@3%Pi-RF-C/AC, 100 nm ZnO@3%PPA-RF-C/AC, and 100 nm ZnO@3%PA-RF-C/AC, were respectively 26%, 25%, and 30% (Figure 1b). For the PA-containing catalyst, the six-membered ring strain and electronic effects stabilize the transition state of the ring structure, reducing the activation energy and accelerating the reaction rate; thus, the catalytic effect of PA is relatively favorable. As seen in Figure 1b, the conversion rates for 100 nm ZnO@3%PPh3-RF-C/AC, 100 nm ZnO@3%HPAA-RF-C/AC, and 100 nm ZnO@3%HEDP-RF-C/AC were 15%, 40%, and 46%, respectively. Introduction of PPh3 into the carbon shell resulted in a low conversion rate, negatively impacting the catalytic activity. However, when HEDP and HPAA were added, the conversion rates notably increased. This enhancement is attributed to the increased adsorption of acetic acid due to the presence of phosphonic acid groups in the catalyst, which improves its catalytic performance. Incorporating substances with phosphonic acid groups into the carbon shell enhances

the catalytic effectiveness; having two phosphonic acid groups in the molecule leads to even better catalytic performance. Therefore, HEDP was selected as the phosphorous source for doping.

Three catalysts, 100 nm Zn/AC, 100 nm ZnO@RF-C/AC, and 100 nm ZnO@5%HEDP-RF-C/AC, were characterized by XPS. Figure 2 shows that the Zn peak intensity decreases when ZnO is coated with resorcinol. After adding HEDP, the ZnO peak intensity decreased again, and a P 2p peak was detected, indicating the successful addition of HEDP to the core-shell structure. The Zn 2p3 spectrum shows that, compared to 100 nm ZnO/AC, the binding energies of Zn 1/2p and 3/2p at 100 nm ZnO@RF-C/AC shift from 1045.17 and 1022.07 eV to 1045.35 and 1022.25 eV, respectively. When HEDP is added, the binding energies shift to higher fields, 1045.70 and 1022.60 eV. That is to say, RF addition leads to a shift in the binding energies of Zn 1/2p and 3/2p to higher fields; these shift even further after HEDP addition, reducing the electron cloud density of Zn [8]. This type of electron transfer facilitates the adsorption of acetic acid onto Zn, i.e., enhances the adsorption of acetic acid onto the catalyst.

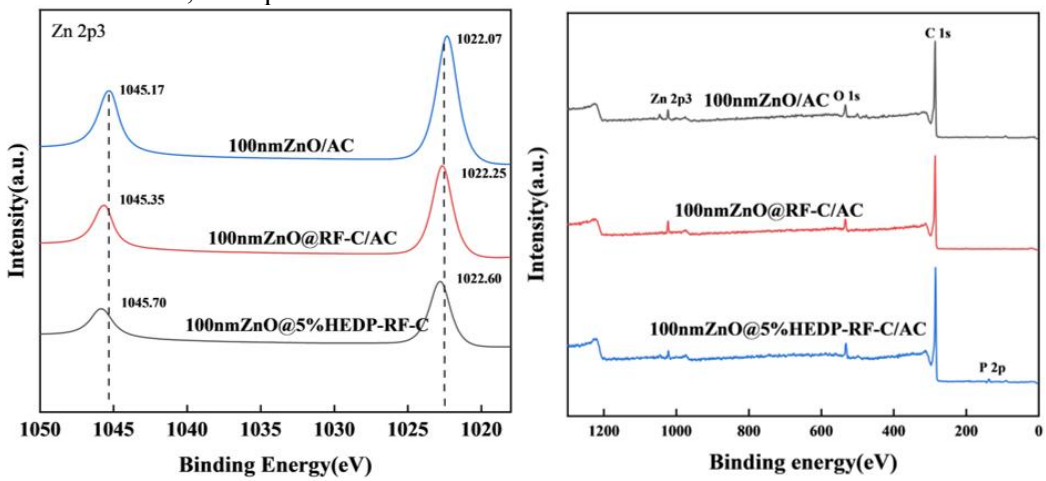

Figure 2. XPS and Zn 2p Spectra of 100 nm Zn/AC, 100 nm ZnO@RF-C/AC, and 100 nm ZnO@5%HEDP-RF-C/AC.

3.2 Performance Evaluation for Different Preparation Conditions

3.2.1 Effect of phosphorous content on the catalyst

The performance of 1%, 3%, 5%, 100 nm 7%, and @10% was assessed. As seen in Figure 3a, the optimal phosphorous content was 5%, for which the catalyst performance reached 53%. Figure 3b presents the XRD patterns of different phosphorous proportions. Diffraction peaks appear at 2θ = 31.776°, 34.419°, 36.260°, 47.543°, 56.610°, 62.858°, 66.394°, 67.959°, 69.103°, 72.559°, and 76.975°. Only ZnO characteristic peaks are present, indicating that the addition of HEDP did not alter the primary phase of ZnO [9]. The addition of P does not alter the morphology of ZnO, but increasing the phosphorus content reduces the intensity of ZnO's peaks. Figure 3e shows the Zn–O stretching vibration at 447 cm^{-1}. This peak decreases with increasing HEDP content, suggesting the successful incorporation of HEDP [10]. When the addition of HEDP reaches over 7%, a P–O stretching characteristic peak appears at 1,078 cm^{-1} [11-13] and becomes more evident when the HEDP content is 10% This demonstrates that HEDP was successfully introduced into the core-shell catalyst, i.e., doped into the catalyst. The nitrogen adsorption-desorption isotherm curves in Figure 3c all show type IV H4 hysteresis loops, which are characteristic of mesoporous materials [14]. The pore structure of the catalyst did not change with the addition of HEDP. As shown in Figure 3d, the pore volume and diameter decreased with increasing HEDP. The optimal performance corresponded to the 5% HEDP addition.

3.2.2 Effect of phosphorous addition sequence on the catalyst

As shown in Figure 4a, the addition of HEDP and hydroquinone led to the optimal performance, reaching 53%. This is because the unpolymerized hydroquinone, a small molecule, possesses high reactivity and readily

undergoes chemical reactions with HEDP, such as the formation of hydrogen or coordinating bonds. Once polymerized, the hydroquinone forms a macromolecular polymer, resulting in reduced reactivity and more stable chemical properties, thus the interactions with HEDP increasingly rely on physical adsorption or surface phenomena. The XRD in Figure 4b indicates that only the characteristic peaks of ZnO are present in the sample, suggesting that the order of phosphate addition does not alter the morphology of ZnO. As illustrated in Figures 4c and 4d, the addition of HEDP and hydroquinone together results in a relatively larger pore structure in the catalyst, thereby yielding the best catalytic performance.

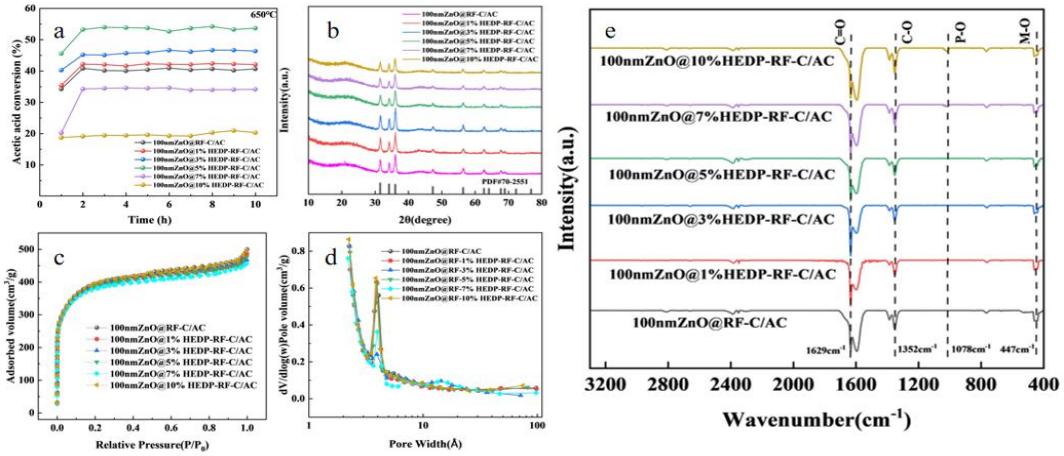

Figure 3. Characterization of the HEDP-RF Doped Catalysts with Different Proportions of HEDP. (a) Catalytic Performance, (b) XRD, (c) and (d) BET, and (e) FTIR.

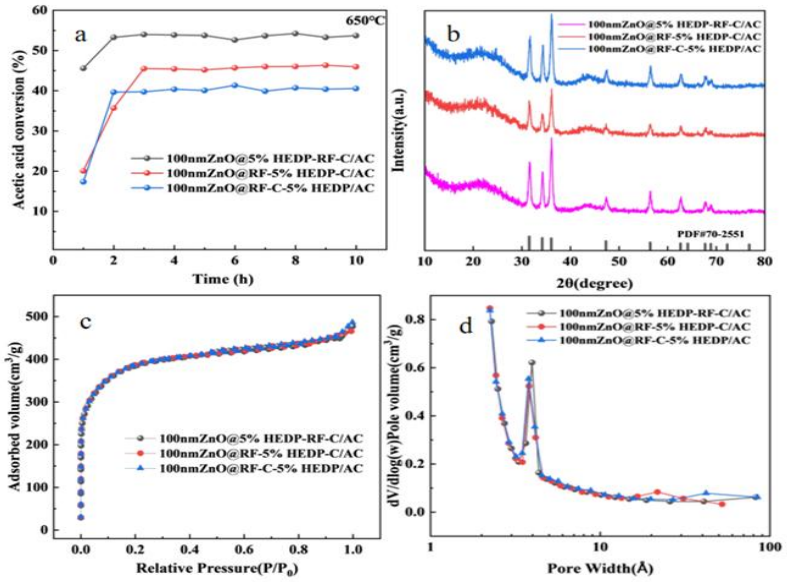

Figure 4. Characterization of the Catalysts Prepared Under Different HEDP Addition Sequences(a) Catalytic Performance, (b) XRD, and (c) and (d) BET

3.2.3 Influence of the calcination temperature on the catalyst performance

Figure 5a shows that the optimal catalytic activity, 56%, was achieved when the calcination temperature reached 650°C. Only the ZnO characteristic peaks were observed in the sample, indicating the absence of other species (Figure 4b). When calcination is not carried out, the zinc oxide peak is weak, because the thickness of the shell affects the diffraction peak. The N_2 absorption and desorption curves shift depending on the calcination temperature (Figure 5c), indicating that calcination affects the catalyst pore structure. Figure 5d shows the pore size distribution of each catalyst; most channels are mesopores. The results reveal that HEDP addition does not change the pore size (Figure 5c), and calcination at different temperatures does not significantly alter the pore size (Figure

5d).

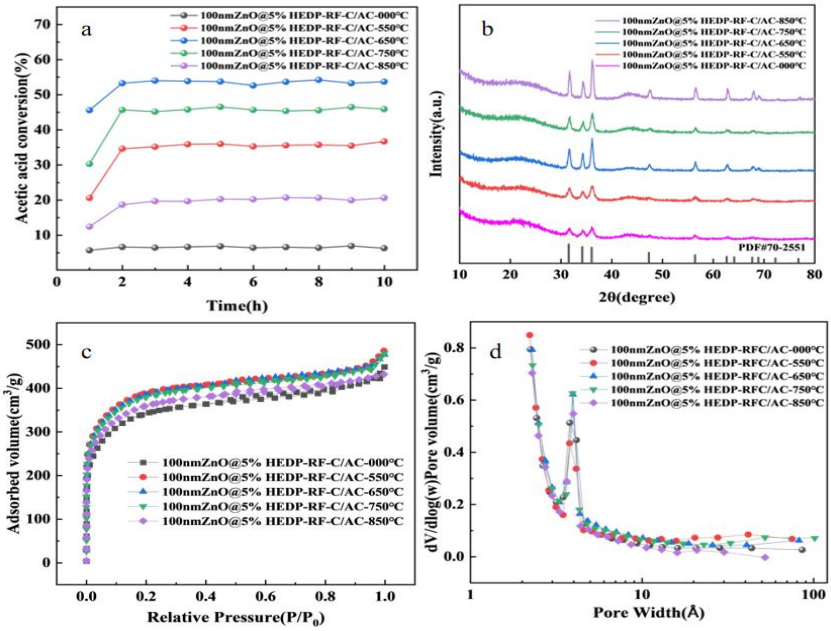

Figure 5. Characterization of the Catalysts Prepared Under Different Calcination Conditions. (a) Catalytic Performance, (b) XRD, and (c) and (d) BET.

3.3 Analysis of the Catalytic Performance

Figure 6a depicts the TEM and SEM images of the 100 nmZnO@5% HEDP-RF-C/AC catalyst, showing that the addition of HPAA does not affect the formation of a core-shell structure. A core-shell structure with well morphology can still be prepared. The lattice fringe of 0.246 nm corresponds to the 101 reflection of ZnO, which is in agreement with the XRD and TEM-mapping results. Figure 6b presents the TEM-mapping characterization of the 100 nm ZnO@5%HEDP-RF-C/AC catalyst.

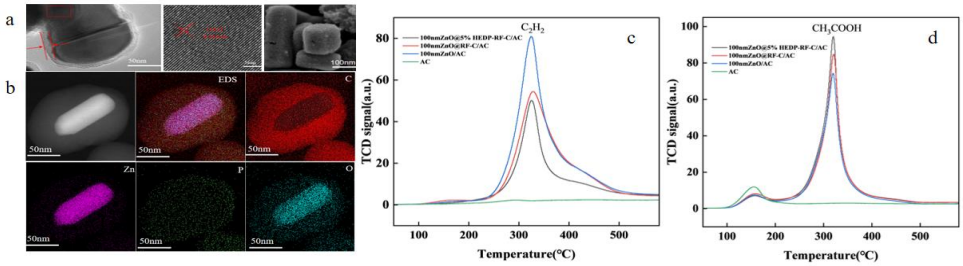

Figure 6. Characterization of 100 nm ZnO@5% HEDP-RF-C/AC by (a) TEM and SEM and (b) TEM-mapping. TPD Adsorption Spectra of (c) C_2H_2 and (d) CH_3COOH.

Table 1. Desorption Temperature of the Reactants and Products with Different Catalysts

Sample	C_2H_2 (°C)	CH_3COOH (°C)
100 nm ZnO@5%HEDP-RF-C/AC	326.32	320.56
100 nm ZnO@RF-C/AC	329.43	320.45
100 nm ZnO/AC	325.96	320.62

The mapping image reveals that ZnO is fully covered by the shell, while the EDS image shows that Zn and O are primarily concentrated in the central region of the core-shell structure, with C present on the outside. Additionally, a few P elements scattered throughout the shell and added to the core can be seen, confirming the successful incorporation of HEDP. This agrees with the XPS and FTIR data in Figures 2 and 3e. The core is composed of ZnO nanoparticles, consistent with the XRD data. From Table 1, it can be observed that the desorption temperature of the reactants and products of the BY catalyst does not vary significantly. Figures 6c and 6d show the peak area representing the adsorption of acetylene and acetic acid, with the abscissa denoting their desorption temperature [15]. As shown in Figure 6c, the peak area of AC is nearly absent, indicating that AC has no adsorption capacity for acetylene.

The catalyst 100 nmZnO/AC has the largest peak area and strong acetylene adsorption,

while 100 nmZnO@5%HEDP-RF-C/AC has the smallest peak area and weak acetylene adsorption. The results for the acetic acid adsorption are the opposite, Figure 6d. 100 nm ZnO@5%HEDP-RF-C/AC has the largest peak area and the best acetic acid adsorption, which is consistent with the XPS results. It can be seen that the addition of HEDP enhances the adsorption capacity of acetic acid and decreases the adsorption capacity of acetylene, which is beneficial for the reaction.

3.4 Analysis of the Catalyst Deactivation

A stability test was conducted for 550 h for the 100 nm ZnO@5%HEDP-RF-C/AC catalyst with the best performance; the results are shown in Figure 7a. After 550 h of reaction, the catalyst activity decreased from the initial 53% to approximately 50%, indicating a slow decline. Table 2 shows the content of Zn in the catalyst before and after the reaction, as analyzed by ICP. Before the reaction, the Zn content was 7.3882%, and decreased to 6.9232% after the reaction with a loss rate of 6.29%. The Zn loss rate for the 100 nm ZnO/AC catalyst after 200 h of reaction was 7.15%. These results indicate that the core-shell structure prepared by coating ZnO with HEDP in RF effectively inhibits Zn loss. However, as shown in Figure 7d, no characteristic ZnO peaks were observed after the reaction, indicating that the active component ZnO was transformed in situ into Zn $(OAc)_2$. BET characterization was performed before and after the reaction. As shown in Figure 7c, the N_2 absorption and desorption curves of the catalyst after the reaction have a much lower specific surface area than before the reaction. Figure 7b shows that the distribution of C, P, Zn, and O is uniform, indicating that ZnO is not coated in a carbon shell. The results show that the carbon shell of the catalyst was broken after the reaction, causing the outward diffusion of Zn and reducing the inhibition of Zn loss. After the reaction, the core-shell structure of the catalyst was destroyed, the pores were blocked, and the specific surface area of the catalyst was affected, leading to a decrease in the reaction activity and stability of the catalyst.

Table 2. Changes in Zn Content Before and After Catalysis

Sample	Fresh (wt%)	Used (wt%)	Zn loss rate (%)
100 nm ZnO@5% HEDP-RF-C/AC	7.3882	6.9232 (550 h)	6.29
100 nm ZnO@RF-C/AC	7.4282	6.9759 (200 h)	6.09
100 nm ZnO/AC	7.5654	7.0245 (200 h)	7.15

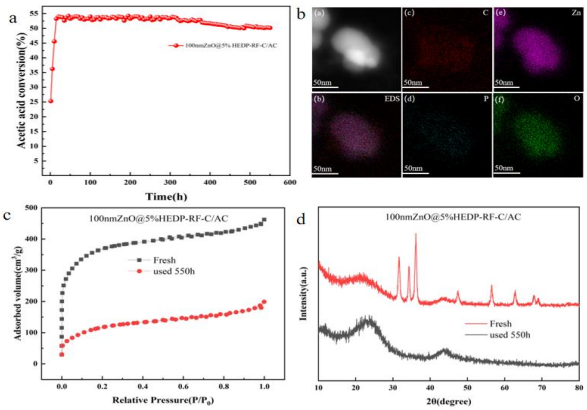

Figure 7. Characterization of 100 nm ZnO@5% HEDP-RF-C/AC. (a) 550 h Stability Test, (b) TEM Distribution of C, P, Zn, and O. (c) BET Pore Size Distribution and (d) XRD Characterization.

4. Conclusions

The efficiency of the core-shell ZnO catalyst was enhanced when doped with hydroxyethylidene diphosphonic acid (HEDP), which contains two phosphonic acid groups. Optimization of the amount of HEDP added, the addition sequence, and the calcination temperature revealed that the best catalytic activity, 53%, was achieved with 5% HEDP added to the RF solution during the preparation of the core-shell structure, followed by calcination at 650°C. The results indicate that the addition of HEDP decreased the electron cloud density around Zn, enhancing the adsorption of acetic acid onto the catalyst and decreasing the adsorption of acetylene. This effect

facilitated the reaction progress and thus improved the conversion rate. Stability tests of the 100 nm ZnO@5%HEDP-RF-C/AC catalyst were conducted and showed that its activity decreased by approximately 3% after 550 h of reaction, with a Zn loss rate of 6.29% (0.011%/h). The Zn loss rates for the catalysts with no phosphorus source and with HPAA were 0.031%/h and 0.025%/h, respectively, indicating that the addition of HEDP can slow down the Zn loss rate. Studies on the catalyst deactivation revealed that blocked pore channels and a lower specific surface area can adversely affect its performance.

Acknowledgments

This research was financially supported by the National Natural Science Foundation of China (22178225).

References

[1] TAZEHABADI M J M, ANSARI M, SABZEVARI A. Controlled synthesis of poly (vinyl alcohol)-poly (acrylic acid) copolymers via cobalt mediated radical polymerization of vinyl acetate initiated by V-70. Journal of Molecular Structure, 2025, 1331: 141637-141637.

[2] ZHANG Y, LI Q, ZHANG Y, et al. Construction of efficient hydrogen evolution catalyst and analysis of the influence of complexing agent type. International Journal of Hydrogen Energy, 2023, 49(PC): 676-688.

[3] MILITZER C, BUCHSBAUM J, DZHAGAN V, et al. Atomic Layer Deposition of Titanium Phosphate from Titanium Tetrachloride and Triethyl Phosphate onto Carbon Fibers. Advanced Materials Interfaces, 2018, 5(16): n/a-n/a.

[4] HUANG J, WANG W, LI H. Water–Medium Organic Reactions Catalyzed by Active and Reusable Pd/Y Heterobimetal–Organic Framework. ACS Catalysis, 2013, 3(7): 1526-1536.

[5] XIANGYU J, BO J, MANRUI M, et al. Complex Core–Shell Architectures through Spatially Organized Nano-Assemblies. ACS Nano, 2025, 3(7): 1526-1536.

[6] YIRAN B, YUNJIAN W, YIBING Y, et al. Unveiling the role of heteroatom doping and strain in Core-Shell catalysts for CO2RR. Chemical Engineering Journal, 2025, 507: 160155.

[7] CHEN Z, ZHAO F, ZHANG H, et al. Effects of trifluoromethanesulfonic acid ligand on the Zinc-based catalysts for the acetylene hydration. Chinese Chemical Letters, 2022, 34(6): 107963.

[8] ZHANG H, XIAO R, LI R, et al. Enhanced aqueous Cr (VI) removal using chitosan-modified magnetic biochars derived from bamboo residues. Chemosphere, 2020, 261: 127694.

[9] QIAN H-S, HAN F-M, ZHANG B, et al. Non-catalytic CVD preparation of carbon spheres with a specific size. Carbon, 2004, 42(4): 761-766.

[10] KRISHNAMOORTHY N, SIVASANKARAPILLAI V S, NATARAJAN V K, et al. Biocidal activity of ZnO NPs against pathogens and antioxidant activity - a greener approach by Citrus hystrix leaf extract as bio-reductant. Biochemical Engineering Journal, 2023, 192: 108818.

[11] YU Y-B, ZHANG Q, WU L-Y, et al. Reaction mechanism of N-(4-hydroxyphenyl) ethanamide electrodegradation via phosphorus-graphene prepared from triphenylphosphine: Generation and destruction of the reactive species. Chemical Engineering Journal, 2020, 403: 126322.

[12] JIANG H, YAN L, ZHANG S, et al. Electrochemical Surface Restructuring of Phosphorus-Doped Carbon@MoP Electrocatalysts for Hydrogen Evolution. Nano-Micro Letters, 2021, 13: 215.

[13] YANG J, GUO D, ZHAO S, et al. Cobalt Phosphides Nanocrystals Encapsulated by P-Doped Carbon and Married with P-Doped Graphene for Overall Water Splitting. Small, 2019, 15(10): n/a-n/a.

[14] GHAFFARIZADEH S A, ZANDAVI S H, WARD C A. Specific Surface Area from Nitrogen Adsorption Data at 77 K Using the Zeta Adsorption Isotherm. The Journal of Physical Chemistry C, 2017, 21(41), 23011-23016.

[15] LI M, XU Z, CHEN Y, et al. MOFs-Derived Zn-Based Catalysts in Acetylene Acetoxylation. Nanomaterials, 2021, 12(1): 98.

